Received: 2 March 2021 | Revised: 22 April 2022 | Accepted: 12 May 2022

DOI: 10.1002/gea.21924

RESEARCH ARTICLE

Geoarchaeology An International Journal WILEY

Mapping magnetism: Geophysical modelling of stratigraphic features by using in situ magnetic susceptibility measurements at Pinnacle Point 5-6 North, South Africa

Ada Dinckal[1,2,3,4] | Erich C. Fisher[5,6,7,8] | Andy I. R. Herries[1,9] | Curtis W. Marean[5,6]

[1]Palaeoscience, Department of Archaeology and History, La Trobe University, Bundoora, Victoria, Australia

[2]Institute for Archaeological Sciences, University of Tübingen, Tübingen, Germany

[3]Departamento de Geografía e Historia, Universidad de La Laguna, La Laguna, Tenerife, Spain

[4]Archaeological Micromorphology and Biomarkers (AMBI Lab), Instituto Universitario de Bio-Orgánica Antonio González, Avenida Astrofísico Francisco Sánchez, La Laguna, Tenerife, Spain

[5]Institute of Human Origins, School of Human Evolution and Social Change, Arizona State University, Tempe, Arizona, USA

[6]African Centre for Coastal Palaeoscience, Nelson Mandela University, Gqeberha (formerly Port Elizabeth), South Africa

[7]Evolutionary Studies Institute and School of Geosciences, University of the Witwatersrand, Johannesburg, South Africa

[8]Interdisciplinary Center for Archaeology and Evolution of Human Behaviour (ICArEHB), Universidade do Algarve, Faro, Portugal

[9]Palaeo-Research Institute, University of Johannesburg, Johannesburg, Gauteng, South Africa

Correspondence
Ada Dinckal, Universidad de La Laguna, IUBO-AMBILAB, Apartado 456, San Cristóbal de La Laguna 38200, Spain.
Email: ada.dinckal@gmail.com

Funding information
John Templeton Foundation; Insitute of Human Origins (IHO); Australian Research Council; Hyde Family Foundation; National Science Foundation

Abstract

This study utilizes geostatistical modelling of magnetic susceptibility (MS) for geophysical prospection of archaeological stratigraphy at the Middle Stone Age rock shelter site of Pinnacle Point 5-6 North. These models are overlaid onto high-resolution photography of the stratigraphic sequence to study the lateral and vertical changes within the magnetic signature of the archaeological sequence and correlate these changes to micromorphological interpretations previously made at the site. In situ analysis is reinforced by laboratory magnetic mineralogical analysis utilizing MS; frequency-dependent susceptibility (χ_{FD}); isothermal remanent magnetization; and anhysteric remanent magnetization to understand the composition of the magnetic minerals creating the in situ signature. This study shows that there is consistent variation in the magnetic signatures of the sequence that can be mapped with in situ MS; there is a correlation with laboratory analysis of magnetic mineralogy, which provides insight into changes in human behaviour; and our models correlate well with micromorphological interpretations of the site.

KEYWORDS

anthropogenic deposits, digital models, environmental magnetics, magnetic susceptibility, Middle Stone Age, Palaeolithic, South Africa

Scientific editing by Dr. Sarah C. Sherwood.

1 | INTRODUCTION

1.1 | Introduction and aims

Environmental magnetism uses mineral magnetic techniques as a proxy for investigating the formation, transportation, deposition and postdepositional alteration of magnetic minerals in sedimentary archives such as lakes and caves (Liu et al., 2012). In archaeology, studies have shown the value of mineral magnetic analysis for reconstructing glacial, interglacial cycling within archaeology-bearing caves (Curnoe et al., 2012; Herries, 2006, 2018; Shipton et al., 2018). Furthermore, studies have also shown the value of mineral magnetic analysis for understanding fire use and occupational intensity in archaeological cave sites (Bradák et al., 2020; Carrancho et al., 2009, 2012, Herries, 2018; Herries and Fisher, 2010; Ozán et al., 2019; Shipton et al., 2018). Meanwhile, climatic studies are based on the transportation and preservation in caves of fine to ultra-fine ferrimagnetic grains (i.e., magnetite or maghemite) that are produced under warm pedogenic processes, but not during cold phases (Herries, 2006; Maher, 1998). Whether a climate signal can be recovered from a cave depends on the source, sediment history and magnetic mineralogy of the sediments (Bradák et al., 2020; Herries, 2018). If the cave is occupied by humans using fire, the sediments are again postdepositionally altered due to the conversion of magnetic minerals by heat. The heating of sediments generally converts weaker ferromagnetic (*s.l.*) grains into stronger ultra-fine ferrimagnetic grains, causing a magnetic enhancement in layers or areas occupied by humans (Herries, 2018; Herries & Fisher, 2010).

Magnetic susceptibility (MS) is an analysis of how easy it is for a material to be magnetized (Dearing, 1999). MS is often used as a first-stage proxy for ferrimagnetic (*s.s.*) concentrations within geological and archaeological deposits; however, it is also sensitive to changes in grain-size variations as well as the types of iron minerals causing the signature (Dearing, 1999; Dearing et al., 1996a, 1996b; Hofmann et al., 2005; Kukkonen et al., 1997; Maher, 1998; Ozán et al., 2019). Previously, MS has been applied with micromorphological analysis as a mechanism of identifying magnetic enhancement in deposits as a proxy for anthropogenic or pedogenic processes (Crowther et al., 1996; Goldberg & Macphail 2012; Herries & Fisher, 2010; Macphail & Crowther, 2007; Macphail et al., 2003; Shipton et al., 2018).

While several studies have looked at vertical variation in MS in archaeological cave sequences (Curnoe et al., 2012; Herries, 2006, 2018; Ozán et al., 2019; Shipton et al., 2018), far fewer have looked at vertical and lateral variations to understand site-use behaviour (Herries & Fisher, 2010). In this paper, we aim to demonstrate that there are consistent vertical and lateral variations in the magnetic signature of the archaeological sequence and that these variations are driven by changes to the magnetic mineralogical composition of the studied areas, which are in turn influenced by anthropogenic actions. We have targeted this analysis at the transition of Marine Isotope Stages (MIS) 5e to 4 at the Middle Stone Age (MSA) site of Pinnacle Point 5-6N (PP5-6N) in the Western Cape province, South Africa. In situ magnetic susceptibility (IMS) is measured across two stratigraphic sequences that occurred during this period of environmental and occupational changes at the site at ~74,000 years ago (ka) (Smith et al., 2018). IMS results are modelled into heat maps; these maps are overlaid onto georectified photomosaics of the archaeological deposits. We demonstrate that the changes in IMS values correspond with changes in the deposits, and by using our in situ modelling, these changes can be associated with changes in anthropogenic deposition. Based on these signatures, we also identify potential anthropogenic layers that have little visible traces of anthropogenic influence. Finally, we utilize bulk samples analysis, gathered from stratigraphically associated deposits during excavation, to provide preliminary magnetic mineralogical context to the changing magnetic signature.

1.2 | Background to magnetic analysis

Anthropogenic-driven combustion can alter the magnetic signature of a deposit. Factors that enhance the anthropogenic magnetic signature include the source of the burnt sediment, with greater enhancement occurring in deposits derived from magnetically weaker rock strata, as well as the temperature of combustion along with the longevity of the process. Furthermore, the amount of oxygen and organic material available while heating will also have an effect (Herrejón Lagunilla et al., 2019; Herries, 2006; Herries & Fisher, 2010; Jordanova et al., 2019). The frequency of repeated burnings will further influence the degree of enhancement and influence the signature (Herries & Fisher, 2010; Herries & Latham, 2009). The close relationship between anthropogenic fire use and magnetic enhancement has allowed for changes in MS measurements as a proxy for human occupation (Herries, 2018; Herries & Fisher, 2010; Shipton et al., 2018). At the MSA site of Pinnacle Point 13B (PP13B), Herries and Fisher (2010) utilized three-dimensional (3D) GIS to study the spatial and temporal distributions of in situ sediment MS values as a proxy for human occupational behaviour and intensity. In similar studies, Herries (2018) and Shipton et al. (2018) have shown that archaeology-bearing cave sites in a wide range of geological settings from Kenya to Australia are applicable to this method, where MS changes and magnetic mineralogy track with occupation intensity when compared to artefact density and fire use.

It is important to note that MS is simply a bulk measurement of magnetization and cannot discern what is generating the signature, be it a natural environmental signature due to sediment influx or human occupation due to fire use. More complex magnetic mineralogical analysis is required to understand the driving factors behind these MS signatures (Dearing, 1999; Thompson & Oldfield, 1986). Along with MS, this paper utilizes frequency-dependent susceptibility (χ_{FD}), isothermal remanent magnetization (IRM) and anhysteretic remanent magnetization (ARM). Progressive IRM curves measure the dominance of ferrimagnetic minerals, such

as magnetite, against anti-ferrimagnetic minerals, like haematite. IRM utilizes a step analysis to incrementally saturate a material to magnetic capacity where ferrimagnetic material will saturate a lot sooner than anti-ferrimagnetic minerals (Evans & Heller, 2003; Tauxe, 2010). Frequency-dependent susceptibility and anhysteric remanent magnetization are used to understand the magnetic domain structures and particle size forming the magnetic signature (Dearing, 1999; Dearing et al., 1996b; Evans & Heller, 2003; Smith, 1999; Tauxe, 2010). Archaeologically, magnetic analysis has been utilized to understand the formation and preservation of a combustion event, which normally produce very fine-grained particles as well as maybe haematite and/or magnetite depending on the atmosphere and prevailing combustion conditions (oxidizing vs. reducing), among other factors. It has further been used to explore postdepositional disturbances that may enhance or remove such particles from a deposit (Bradák et al., 2020; Carrancho & Villalaín, 2011; Carrancho et al., 2009; Dearing, 1999; Dearing et al., 1996b; Herries, 2006; Herries & Fisher, 2010; Jordanova et al., 2019).

1.3 | Pinnacle Point 5-6 North

Pinnacle Point 5-6 North (PP5-6N) is one of numerous coastal sites located at Pinnacle Point in the Western Cape Province of South Africa (Marean et al., 2004; see Figure 1). These sites have been the focus of intense study by the South African Coastal Paleoclimate, Paleoenvironment, Paleoecology, and Palaeoanthropology Project (SACP4). The excavations at PP5-6N and other sites have provided important information about the evolution of modern human behaviours, including the earliest evidence of the systematic exploitation of coastal resources (Marean et al., 2007), stone tool heat treatment (Brown et al., 2009), microlithic technology (Brown et al., 2009, 2012) and the influence of the Toba supervolcano on African hunter-gatherers (Smith et al., 2018).

Site PP5-6N is a ~15 m stack of sediments within a coastal rock shelter that alternates between anthropogenic- and geogenic-dominant deposits. These deposits have been revealed via a 20 m 'Long Section' excavation trench running parallel to the rock. Aeolian dune deposits are present at the base of the Long Section, with the

FIGURE 1 Location of the Pinnacle Point cave complex as well as PP5-6 and PP-13B. [Color figure can be viewed at wileyonlinelibrary.com]

archaeological sequence overlying it. This dune is recognized at several other caves across the PP complex (Karkanas et al., 2015) and has been dated at PP5-6N and other sites to ~90 ka (Bar-Matthews et al., 2010; Jacobs, 2010). The youngest deposits at PP5-6N have been dated to around ~50 ka (Brown et al., 2012; Smith et al., 2018). The archaeological sequence within this 40,000-year period spans interglacial MIS5, glacial MIS4 and early MIS3 (Brown et al., 2012; Karkanas et al., 2015; Smith et al., 2018).

The excavation methodology at Pinnacle Point groups large bodies of mostly homogeneous sedimentary types into 'Stratigraphic Aggregates' (StratAggs). This study targets two of these StratAggs: the Ashy Light Brown Sand (ALBS), a 0.7 m thick unit composed of rich aeolian white sand with trampled combustion features, and the Shelly Ashy Dark Brown Sand (SADBS), which is 0.8 m thick primarily defined by combustion features intermixed with both beige and white aeolian sands (Karkanas et al., 2015).

The importance of the ALBS and SADBS lies in the transition from MIS5e to 4 and documents several interesting changes in human behaviour, such as an increase in the use of silcrete and the appearance of microliths in early MIS4. The ALBS and SADBS are dated concordantly with both optically stimulated luminescence (OSL) methods and the finding of the Younger Toba Tuff (YTT) through cryptotephra analysis in the ALBS (Smith et al., 2018). Identification of the YTT at Pinnacle Point has provided the first direct evidence of YTT in an African archaeological deposit. Although the influence of YTT is still unknown, what is observable is the continuous hunter-gatherer occupation of the site across the YTT isochron (Smith et al., 2018).

The ALBS and SADBS also document the recession of the coastline as sea levels dropped with the transition from MIS5e to 4. These changes exposed the shallow and flat Agulhas Bank directly offshore to Pinnacle Point, leaving the site stranded up to 22 km from the coastline (Fisher et al., 2010). These environmental changes are also reflected in the transition of the roofspall heavy deposits of the Strataggs below ALBS into the aeolian-driven deposits of ALBS (Karkanas et al., 2015; Smith et al., 2018). The aeolian deposits are composed of beige sand facies. These facies have little chemical alteration and do not preserve intense stratification as is found at aeolian deposits preserved elsewhere at Pinnacle Point. The absence of this stratification has been linked to anthropogenic activities such as levelling and flattening of the surfaces (Karkanas et al., 2015). Experimental work conducted during the 2010 study at PP13B showed that these aeolian quartz sand deposits are weakly magnetic and are dominated by diamagnetic components (Herries & Fisher, 2010; SOM). ALBS preserves one dense unit of anthropogenic accumulation with combustion features, called the 'Conrad Shell', as well as several thin lenses of human occupation (Smith et al., 2018). Below the 'Conrad Shell' is the aeolian deposit called the 'Conrad Cobble and Sand', and above the 'Conrad Shell' is the aeolian deposit called the 'Conrad Sand' (Smith et al., 2018). The 'Conrad Sand' leads into the palimpsest of trampled combustion features that is the SADBS. The combustion features of the SADBS lay horizontally, flattened due to either frequent movement over the habitational surface or intentional surface flattening, with alternating layers of sand-rich ash microfacies (MF) and occasional pure ash MF. Single depositional hearths are not discernible in the SADBS; instead, the formation is composed of cumulative palimpsests (Karkanas et al., 2015). These combustion palimpsests further align with an increase in the density of artefacts (Smith et al., 2018).

2 | METHODS AND SAMPLING

2.1 | Sampling

The ALBS and SADBS deposits are located between 5 and 7 m below pedogenically altered topsoil; this avoids the potential magnetic enhancement or alteration that may occur due to secondary pedogenic overprinting (Herries & Fisher, 2010). Both deposits are composed primarily of sands that vary from a primarily diamagnetic (low magnetic) beige sand with minimum chemical alteration in ALBS, to white ashy sands in SADBS that are likely to be magnetically enhanced through thermal alteration (Karkanas et al., 2015; see Herries & Fisher, 2010 for magnetic analysis of dune deposits at Pinnacle Point 13B). Due to the weak and diamagnetic nature of the geogenic dune sands, variations in iron concentration and ash composition, dispersion and concentration should be visible through a high-resolution IMS study.

Water has left a very clear mark on numerous deposits at PP5-6N, being most evident in an ancient drip line that cut its way across portions of the excavated deposits (Karkanas et al., 2015). Karstic or pseudokarstic movement of water through caves and sediment has been shown to impact magnetic signatures in deposits where water logging has occurred. Dissolution of iron, particularly concentrations of fine-grained magnetite, removes iron minerals from the deposit, lowering the MS values (Herries & Latham, 2009). Fortunately, both ALBS and SADBS are located fully behind the past and present drip line of the cave, protecting these deposits from external alteration processes (Karkanas et al., 2015).

Laboratory analysis was conducted to understand the different magnetic mineralogical compositions that could form the magnetic signature identified in the IMS models, as well as providing an insight into the variation within magnetic values across the studied area. Samples for laboratory analysis were selected from referential bulk samples gathered during the excavation of individual stratigraphic units from ALBS and SADBS. Selected samples were not directly aligned with profiles sections mapped out with IMS, but are from stratigraphically linked excavated units during the 2012–2014 field seasons and could be from several metres away from the location of the IMS models. Samples were prepared postfield season. Using a 3-mm sieve, fine sediment was separated from coarse material that may dilute the magnetic signature. The fine sediment was left to dry for 48 h before being packaged into a standard-sized palaeomagnetic sampling cube, around 8 cubic centimetres in volume. Samples were then weighed, and measurements were corrected for weight to produce mass-corrected MS values, identified by the symbol χ

(Dearing, 1999). A total of 139 samples were measured for their frequency-dependent susceptibility (χ_{FD}). Of these 139 samples, 10 were selected for progressive IRM curves and ARM analysis. These 10 samples were selected to provide the largest range of MS signatures to categorize for their magnetic mineralogy. Laboratory analysis followed the procedure of preforming dual frequency MS first, followed by ARM analysis and finally progressive IRM curves. All laboratory analyses were conducted in the Australian Archaeomagnetism Laboratory (TAAL), at the University of La Trobe, Australia. Statistical analysis and graphs were produced with R and ggplot2 (Team R. Contributors, 2021; Wickham, 2016).

2.2 | Model creation

IMS surveying was conducted using the Bartington MS2 Magnetic Susceptibility Metre with an attached MS2K-probe. The MS2K-probe provides surface measurements across a ~25 mm diameter area. The sensitivity of the MS2K-probe retrieves 100% of the signature in the first millimetre, and up to 50% of the signature at 3 mm of penetration. The smallest measurement achievable by the probe was 1×10^{-6} (S.I. units), and therefore, anything lower than this value would be beyond the sensitivity of the machine and register as a value of zero (see Bartington Instruments, 2019; Operation Manual for MS2 Magnetic Susceptibility System). MS values were measured by the MS2K-probe as volume susceptibility (κ) at S.I. units of 10^{-5}. Profile sections were cleaned both before excavation at the start of the field season and once more immediately before sampling was undertaken. The sampling of the profile sections was taken in vertical transects. The average distance between each sampled location was ~2.5 cm; however, sampling resolution was also refined to a minimum distance of 5 mm to capture sharp transition from one stratigraphic unit to another and to assure that all stratigraphic units were sampled in areas where stratification of the profile was more intense. The MS2 was set on the continuous measurement setting and an air measurement was taken between each sediment measurement to control for drift. The metre was zeroed after five measurements or any anomalous drift. A single measurement was taken at each location; however, if a measurement seemed anomalous, repeated measurements were taken after calibration and zeroing of the machine. Assuming no instrumental error explained the anomalous result, the first measurement is utilized. Figure 2a shows the distribution and range of IMS measurements gathered in the field. Across the two sections, a total of 1062 measurements were taken. Five-hundred and thirty five measurements were taken from the ALBS section, with a mean value of 27.49×10^{-5} (S.I.). Five-hundred and twenty seven measurements were taken from the SADBS section, with a mean value of 64.76×10^{-5} (S.I.). Raw data are provided in the Supporting Information Material.

The raw IMS data provide measures of discrete points as measured by the MS2K-probe. While discrete IMS point measurements can reveal patterns within the data set, it forces a categorical representation to the data belying the actual continuous distribution of MS within the sediments. There are two ways to model discrete point sets continuously. Deterministic methods are an exact interpolation technique that projects a surface through a set of points based on the degree of smoothing or similarity. In contrast, geostatistical methods rely on the spatial autocorrelation of known points to predict values at unknown locations and assess the uncertainty of these predictions. In this situation, spatial autocorrelation refers to the distance between two measured points and the difference between their MS values. The MS values of nearer points are assumed to be more closely related than more distant points and variography defines the way in which this relationship decreases over distance. A key benefit of geostatistical methods is the ability to assess the uncertainty (variability) associated with the predictions.

We used the ESRI ArcGIS Pro 2.4 Geostatistical Analyst to model each section. For each section, we first explored quantile–quantile plots of the IMS values to determine if they were normally distributed or not, potentially requiring a transformation to make the point values normally distributed; this was not required. Thereafter, different kriging modelling methods and semi-variograms were tested. Before modelling each section, we extracted a randomized 10% sample of raw data from each data set. This sample was set aside to test the robustness of the geostatistical models after they were created.

An ordinary kriging model provided the best results for the lower profile (Figure 2c,e), which sampled within the largely low MS ALBS. Untransformed data provided the best results, and an exponential semivariogram provided the smallest mean (−0.0970) and standardized mean (−0.0067). The root-mean-squared prediction errors were also low (15.8138) and only differed from the average standard errors (15.6859) by a value of 0.0128, which suggests that the model accounted for the variability within the data in the model predictions. After the model was created, it was validated using the 10% subset of points removed before analysis. The absolute difference between the 10% subset of MS points had a mean absolute error of 10.768. The south 844.5 profile from west 727.5 to west 726, however, crossed the ALBS/SADBS boundary and had a much larger range of MS values. To model this section, we utilized Empirical Bayesian Kriging (EBK) regression prediction. EBK differs from other kriging methods by estimating the error of the semivariogram that is used to measure spatial autocorrelation within the data. EBK regression prediction can also change the model to account for local effects.

In the higher profile (Figure 2b,d), the three distinct units (Figure 2d; Conrad Sands, Jocelyn and Erich) have increasingly higher MS values up the section (Table 1). By utilizing subset polygons based on these unit boundaries, it improved the model performance compared to using a single model across the entire data set.

A K-Bessel semivariogram model across 1000 simulations provided the best results. The average Continuous Ranked Probability Score was 13.7667, suggesting low deviations between the observed data values and the predictive cumulative distribution. The mean and mean standardized values of 0.1205 and 0.0139, respectively, indicated unbiased prediction errors. The root-mean-

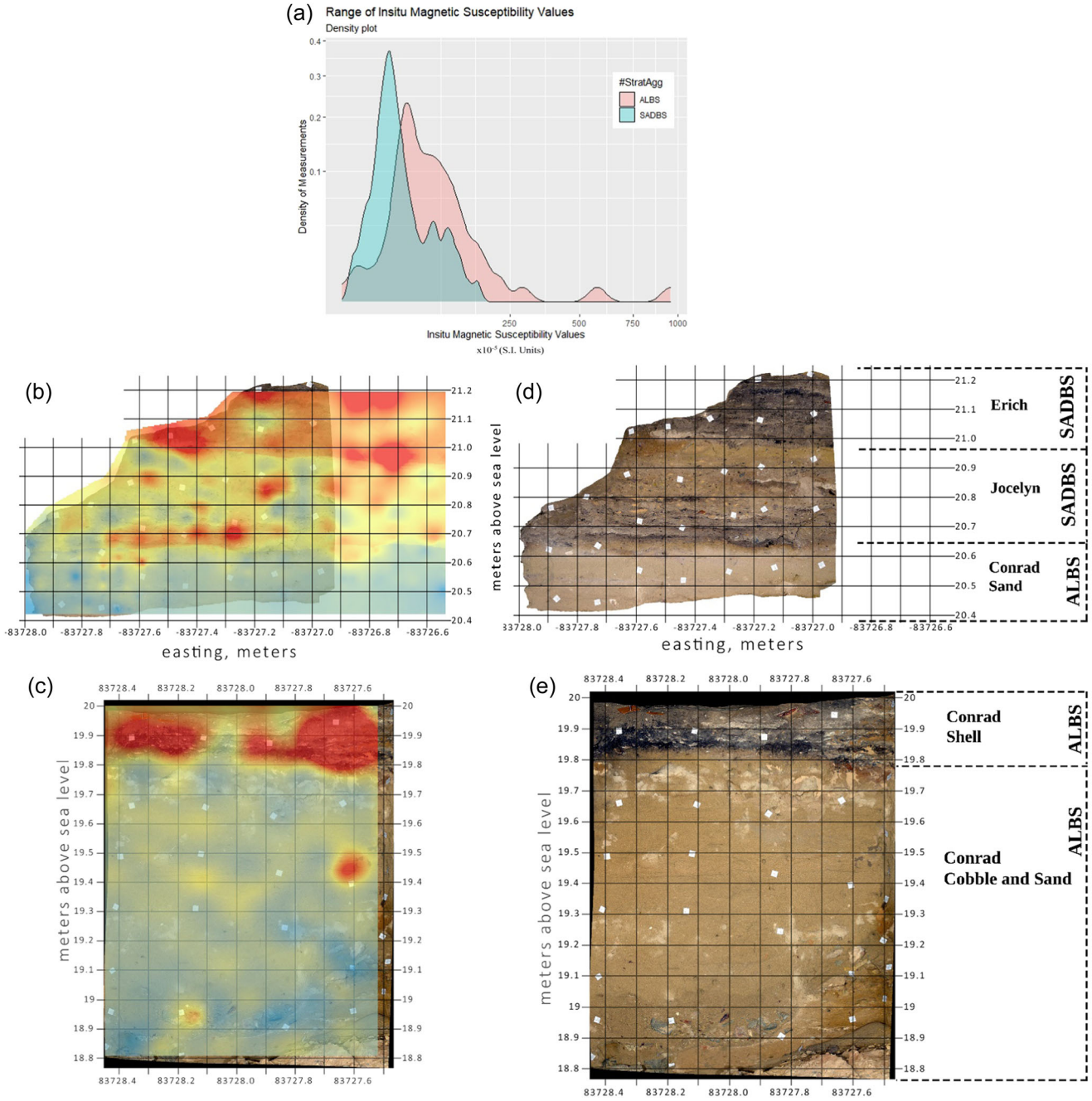

FIGURE 2 (a) The range and distribution of in situ magnetic susceptibility (IMS) used within the models. The scale of the *x*-axis was subjected to a square transform to better highlight the distribution of the lower values. The scale of the *y*-axis was also subjected to a square transform to highlight the presence of the higher values and show the complete range of IMS values. (b) Photomosaic and in situ magnetic susceptibility mapping of SADBS. (c) Photomosaic and in situ magnetic susceptibility mapping of ALBS. (d) Photomosaic of upper ALBS and SADBS with stratigraphic units associated with ALBS and SADBS highlighted. (e) Photomosaic of ALBS with stratigraphic units highlighted. A total of 1062 measurements were taken across the two sections of the SADBS and ALBS. Five-hundred and thirty-five measurements were taken from the ALBS section with a range of 1.00–160.00. The ALBS section presented here is ~1 m wide (East–West extent) and ~1.2 m tall. Five hundred and twenty-seven measurements were taken from the SADBS section, which has a range of values from below the sensitivity of the equipment to 956.00×10^{-5} (S.I. units). SADBS is ~1.5 m wide at its greatest extent and ~0.80 m tall at its highest. ALBS, Ashy Light Brown Sand; SADBS, Shelly Ashy Dark Brown Sand. [Color figure can be viewed at wileyonlinelibrary.com]

squared prediction error was 27.479, but it only differed from the average standard error (27.0675) by a value of 0.412, which suggests that the model accounted for much of the variability within the data in the model predictions.

After the model was created, it was also validated using its 10% subset of points removed before analysis. The subset of MS points and the results of the model had a mean absolute difference of 13.44.

TABLE 1 MS values identified per stratigraphic unit demonstrating the increase in the average MS values throughout the profile.

SubAgg	Average MS ($\times10^{-5}$)	Min MS ($\times10^{-5}$)	Max MS ($\times10^{-5}$)	Std. dev. MS ($\times10^{-5}$)
SADBS Erich	95.85	9	220	38.80
SADBS Jocelyn	67.67	0	287	38.93
ALBS Conrad Sands	40.13	1	118	15.35

Note: It is noteworthy that while the highest maximum MS is in SADBS Jocelyn, the highest averages are found through SADBS Erich.
Abbreviations: ALBS, Ashy Light Brown Sand; MS, magnetic susceptibility; SADBS, Shelly Ashy Dark Brown Sand.

2.3 | Equipment and method: MS

MS characterizes the ease with which a material can be magnetized (Dearing, 1999). Frequency-dependent susceptibility (χ_{FD}) identifies the domain structures of magnetic minerals by comparing the MS of magnetization at two frequencies: a low frequency (χ_{LF}) of 0.46 kHz and a high frequency of 4.6 kHz (χ_{HF}). As the frequency of an applied field increases, the impact of finer grains on the MS decreases. Therefore, higher concentrations of fine to ultra-fine-grained magnetic particles will lead to a lower χ_{HF}. The ratio between the two measurements can be used to identify the dominant domain structure of the material. Subsequently transforming these measurements into percentage ratios can quantify these changes (Dearing, 1999; Thompson & Oldfield, 1986). Generally, very low χ_{FD}% (<1%) is characteristic of multidomain grains; χ_{FD}% of 1%–7% denotes higher concentrations of single-domain (SD) structures, although concentrations of fine to ultrafine superparamagnetic (SP) grains may also be present. χ_{FD}% above 7% marks the increase in concentrations of fine to ultrafine SP grains, with values above 10% being primarily composed of these fine SP minerals (Dearing, 1999). A Bartington MS2 Magnetic Susceptibility Meter and a Bartington Dual Frequency MS2B Sensor were utilized in the measurement of susceptibility in the laboratory. MS measurements are presented in mass-corrected values for χ_{LF} and χ_{HF} at SI units of $\times10^{-8}$ (m^3/kg), while χ_{FD}% are calculated using the equation $\chi_{FD}\% = ([\chi_{LF} - \chi_{HF})/\chi_{LF}] \times 100$; specification in Dearing, 1994; Dearing et al., 1996a).

2.4 | Equipment and method: IRM and ARM

IRM is used to identify the different iron oxides. IRM analysis is done by magnetizing the material with an applied field (*H*) that grows incrementally in strength. Ferrimagnetic minerals such as magnetite or maghemite saturate much faster (<300 mT) than anti-ferrimagnetic minerals such as haematite and goethite (~3 T). These saturations can be identified by plotting the saturation onto a graph and observing the curve (Robertson & France, 1994). IRM analysis was conducted on a Magnetic Measurements MMPM10 9 T pulse magnetizer. Remanence measurements were made after each IRM step on the JR6 Magnetometer. While samples were mostly saturated at values before 300 mT, for purposes of normalization and standardization of the data saturation IRM (SIRM), values were obtained at measurements of 800 mT.

ARM is a method of inducing magnetic remanence without a magnetic hysteresis (anhysteretic remanence). An anhysteretic remanence shows a distinct relationship with grain size, especially for iron minerals such as magnetite, and has been used as a grain size indicator (Evans & Heller, 2003; Smith, 1999). An ARM is a single measurement value that is induced by applying a small direct current biasing field while demagnetization is performed by an alternating field (AF). As the field intensities decrease, the magnetite grains have a statistical preference for the biasing field, because small particles (especially SD or pseudo-SD grains) are more efficient at acquiring a remanence and will yield higher values, thus being useful in identifying grain size (Evans & Heller, 2003; Tauxe, 2010). ARM analysis and sample demagnetization were conducted using an AGICO PAMI Anhysteretic Magnetizer. Samples were measured using an AGICO JR6 Spinner Magnetometer. Before inducing the ARM, samples were demagnetized to 200 mT with an AF demagnetizer to remove any previously acquired magnetic remanence. The new remanence was induced by subjecting the samples to an AF of 100 mT and a biasing field of 40 μT. The IRM and ARM values are provided in *A*/*m* units.

2.5 | Wood-ash experiment

An opportunistic experimental analysis of potential local combustion fuel sources was undertaken before this study and at the same time as the work published in Brown et al. (2009) and Herries and Fisher (2010). While undertaking the work for these papers, it was noted that some wood ash was very weak, while other wood ash was magnetically very strong and that this seemed to vary according to the type of wood used, mostly the nonindigenous red-eyed wattle (Rooikrans) and Namibian hardwood. To test why this was the case and weather local woods also showed similar variability, a series of experimental burns were conducted to create wood ash from different tree species and different parts of the tree (i.e., bark vs. wood core). While some work has been done to identify different magnetic characteristics of highly variable fuel sources in a European context such as peat versus wood ash (Church et al., 2007),

these studies have not looked at whether different wood species would create different magnetic characteristics, or what drives such variability. These data provide some contextual information regarding the varying nature of ash derived from local fuel sources. A complete description of the methods and results for this experiment can be found in the Supporting Information Material (wood-ash experiment).

3 | RESULTS

3.1 | Models

3.1.1 | ALBS

Two distinct stratigraphic units belonging to the ALBS, the 'Conrad Cobble and Sand' and the 'Conrad Shell' combustion feature, are represented in Figure 3 (see Figure 2e for unit boundaries). Our models show that these units have distinctively different magnetic signatures. The boundary between these two depositional units occurs at 19.8 m above sea level (masl) in Figure 3. Below this boundary are the aeolian sand deposits called the 'Conrad Cobble and Sand'. In our model (Figure 3), the ALBS 'Conrad Cobble and Sand' are visible as a mottled layer, with low to moderate IMS values (blue; low IMS values begin at 1.00×10^{-5}, grading into yellow; moderate IMS values from around $\sim 66 \times 10^{-5}$ to $\sim 100 \times 10^{-5}$). The low IMS values are due to the overall weak and diamagnetic nature of the aeolian sand that has been identified through experimental work on other aeolian dunes at Pinnacle Point (Herries & Fisher, 2010; SOM). The mottled nature of moderate values is therefore a deviation from the expected low IMS values. The highest concentration of moderate IMS values is present from elevations of 19.4–19.7 masl. At Pinnacle Point 13B, it has been shown that anthropogenically driven mixing of combustion material does occur in occupational areas without identifiable combustion features (Herries & Fisher, 2010). In part, this is due to the way in which sandy deposits are moved around the cave floor by human and animal movements, which disturb and redistribute ephemeral combustion features. Human occupation occurring elsewhere on the site can distribute ferric material through nearby campfire smoke, or simply through dispersal of hearth residue through the movement of people around the occupational area. This can explain the inflation of IMS values in areas that appear to be composed of low magnetic aeolian sands.

Within these deposits are a variety of IMS hot spots. One of these hot spots, IMS values $\sim 95 \times 10^{-5}$, occurs at around 18.95 masl and easting −83,728.15 m. The second hot spot, IMS of $\sim 120 \times 10^{-5}$, can be seen at 19.45 masl and eastings −83,727.6 m. The first hot spot (at 18.95 masl) is associated with a band of roofspall visible within the photomosaic as a sloping sequence of gravel to palm-sized rocks interlaced with the aeolian sands and is composed of low IMS values, while the second hot spot is located within the most mottled components of the 'Conrad Cobble and Sand'. The causation of either hot spot has not been identified; however, the 'Conrad Cobble and Sand' have been noted to have several discrete lenses of human occupation that these hot spots may represent (Smith et al., 2018). The aeolian sand deposits within the 'Conrad Cobble and Sand' show little to no evidence for chemical alteration (Karkanas et al., 2015), so a nonanthropogenic cause for these hot spots would not be likely.

The dominant beige sands transition to the white ash, and sand-rich ash MF of the 'Conrad Shell', which is the ALBS single largest occupational deposits (Karkanas et al., 2015; Smith et al., 2018). These deposits are described as a sand-rich ash MF, which is aeolian sand embedded within a dense matrix of reworked ash mixed with charred material, exfoliated shell fragments and burnt bone. The IMS model is not able to distinguish between these two layers of ash-rich deposits, but does show distinct high (>100) IMS values as expected for such a dense combustion feature.

The final deposits of the ALBS are shown in the Figure 4 model, from elevations of 20.4–20.65 masl (see Figure 2c for boundaries). This is the final aeolian deposition of the ALBS called 'Conrad Sand'. There is little anthropogenic alteration or input here, which is highlighted by the almost homogeneous distribution of low IMS values throughout this deposit.

3.1.2 | SADBS

The transition from the 'Conrad Shell' to the SADBS combustion features is captured at 20.65 masl (Figure 4b) and represents the transition from the aeolian sand of ALBS into the ashy rich cumulative combustion feature palimpsest of SADBS. The contact between ALBS and SADBS is not as defined as the combustion features in the ALBS. In Figure 4d, the values range from the low IMS values (blue values until $\sim 70 \times 10^{-5}$) of the Conrad Sand to a mottle of moderate values (yellow values from $\sim 70 \times 10^{-5}$ to $\sim 100 \times 10^{-5}$) and high values (red values from 100×10^{-5} and higher) of the SADBS combustion features. This mottled composition of moderate to high values spans from elevations of 20.65–20.95 masl.

The lower portions of the SADBS (called Jocelyn, Figure 2d) have been noted to have a higher frequency of sand than the higher portions of the deposits (called Erich, Figure 2e) (Karkanas et al., 2015; Smith et al., 2018). This would explain the moderate values within the lower SADBS, Jocelyn, when compared to the dominantly high IMS values above in Erich.

Within the region of mottled moderate to high values of Jocelyn, there are two horizons of moderately high to high IMS values (Figure 4d). When comparing the photomosaics with the models (Figure 4d,c), it becomes clear that these horizons are associated with horizontally laid deposits. The first is at 20.7 masl, with high values located in a horizon between eastings of −83,727.0 to −83,727.8 m. The second is at 20.85 masl, with fragments of high values located at eastings of −83,727.8, −83,727.2 to −83,727.1 and −83,727.0 to −83,726.6 m. Bioturbation has been identified as impacting Jocelyn

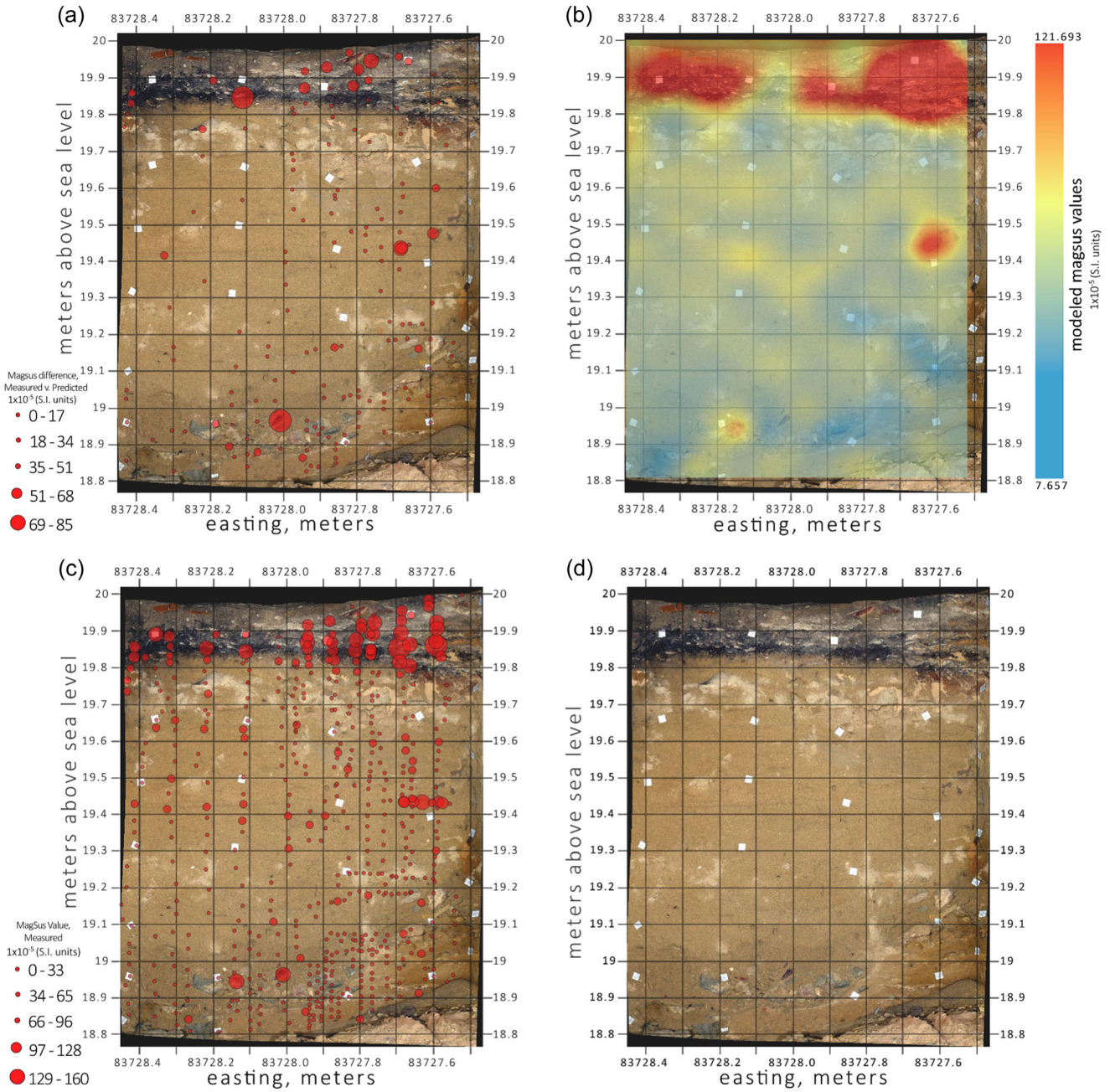

FIGURE 3 ALBS models. (a) Absolute difference between the 10% training points withheld from modelling and the interpolated model values. (b) The geostatistical model showing the continuous modelled distribution of magnetic susceptibility across the stratigraphic section. (c) The location of all in situ magnetic susceptibility points. The scale is proportional from 100% of the maximum value to 1% of the maximum value. (d) High-resolution photomosaic of the ALBS. For each panel, vertical gridlines represent orthometric height in metres, while horizontal gridlines represent South African National Grid coordinates (Lo.23) in metres. The ALBS was mapped out with 535 measurements that covered a range from 1.00×10^{-5} (S.I. units) to 160.00×10^{-5} (S.I. units). The ALBS has a mean of 27.49×10^{-5} (S.I. units) and a median of 21.00×10^{-5} (S.I. units). 72.5% of the values fall below the mean and 55% are below the median. 90.0% of the values fall below 58.00×10^{-5} (S.I. units), while the last 10.0% extends from 58.00×10^{-5} (S.I. units) through to 160×10^{-5} (S.I. units). ALBS, Ashy Light Brown Sand. [Color figure can be viewed at wileyonlinelibrary.com]

(Karkanas et al., 2015), which is reflected in the models. The mottling of the high values of this sequence is likely a product of this bioturbated mixing, with the increased sand mixture further lowering the IMS values, while the fragments of solid high IMS horizons are remnants of deposits that have not been impacted as thoroughly by the bioturbation.

In Erich, the IMS models are more homogeneous in their high values (Figure 4d). This is likely due to these deposits appearing to be less disturbed, along with the decrease in the frequency of sand and more intact combustion material, as seen by the solid black deposits and repeated thin ash lenses in the photomosaics.

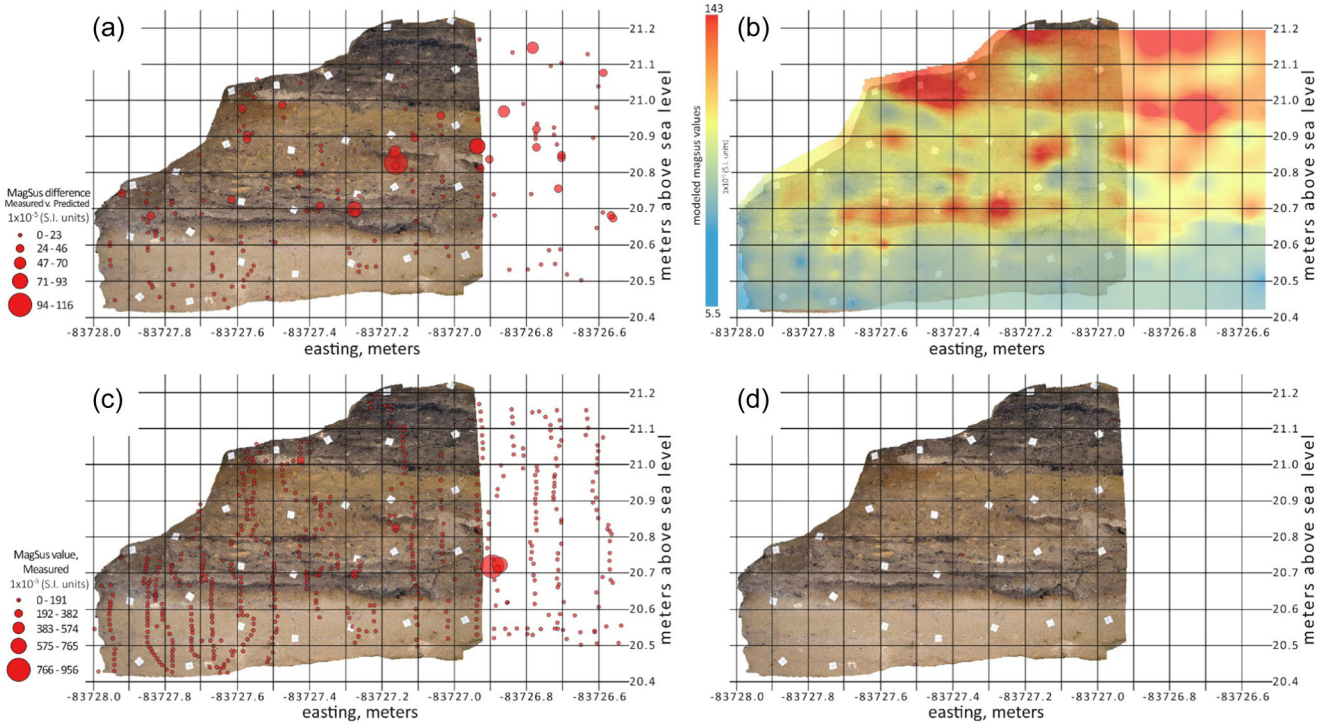

FIGURE 4 SADBS model. (a) Absolute difference between the 10% training points withheld from modelling and the interpolated model values. (b) The geostatistical model showing the continuous modelled distribution of magnetic susceptibility across the stratigraphic section. (c) The location of all in situ magnetic susceptibility points. The scale is proportional from 100% of the maximum value to 1% of the maximum value. (d) High-resolution photomosaic of ALBS to SADBS transition at elevations of 20.65 and lower shows the final deposits of the ALBS. Above 20.65 is the SADBS. For each panel, vertical gridlines represent orthometric height in metres, while horizontal gridlines represent South African National Grid coordinates (Lo.23) in metres. These models were mapped out with 527 measurements that had a range below the sensitivity of the equipment to 956.00×10^{-5} (S.I. units). The mean was 64.76×10^{-5} (S.I. units), and the median was 49×10^{-5} (S.I. units). A total of 62% of the values fall below the mean, while 50% of the values fall below the median. About 90% of the values fall below 111, while the last 10% are between 111×10^{-5} (S.I. units) and 956×10^{-5} (S.I. units). However, in the models depicted here, extraordinarily high values over 333×10^{-5} (S.I. units) were not used so as not to skewer the values generating the model. These values were a very small component of the section, and their removal does not impact the results. ALBS, Ashy Light Brown Sand; SADBS, Shelly Ashy Dark Brown Sand. [Color figure can be viewed at wileyonlinelibrary.com]

3.2 | Laboratory analysis

3.2.1 | Laboratory MS results

Table 2 presents the breakdown of results for samples that were subjected to laboratory analysis. Raw data are available in the Supporting Information Material. The laboratory analysis of magnetic mineralogy shows that there is a very large range in MS throughout ALBS and SADBS (Table 1), as identified in the IMS models, which can be driven by a variety of different mineralogical compositions. The results (Figure 5) show that the deposits generally have high χ_{FD}% values between 5% and 10% (Figure 5b) that consist of fine to an ultra-fine SD (25–80 µm in size for magnetite grains) to SP (~0.01–0.03 µm for magnetite grains) grain sizes (Dunlop & Özdemir, 1997). There is no definitive trend between χ_{LF} and χ_{FD}%. Low χ_{LF} values, under $50 \times 10^{-8}\ m^3\ kg^{-1}$, have a χ_{FD}% range between 1% and 11%. Higher values tend to have a reduced range of around ~8%. This is quite typical of archaeological deposits in South Africa and is in part due to concentration effects in different types of deposits (Herries & Latham, 2009). A small amount of ferric burnt material, such as ash or heated sediment, in low magnetics sands will have a low χ_{LF}, but will still produce a higher χ_{FD}% due to the presence of ultra-fine-grained ferrimagnetic material dominating the signature, whereas sediments that have not been burnt will have higher χ_{LF} values, but lower χ_{FD}% values (Herries & Latham, 2009).

3.2.2 | Systematic error in frequency-dependent results

Figure 5a,b, shows how the results differ between MS at low- and high-frequency magnetic fields, that is, the χ_{FD}. Figure 5b shows that there is a low correlation (Pearson's correlation of 0.118) between the χ_{LF} and χ_{FD}%, indicating that an increase in χ_{LF} does not automatically mean an increase in χ_{FD}% and that other factors drive a change in MS. However, χ_{FD}% does correlate highly with χ_{HF} (Pearson's correlation of 0.861). While this could be a characteristic of the grain size relationship with MS on the site, χ_{FD}% can be influenced by a systematic error occurring when the sensitivity of the

TABLE 2 Statistical summary of laboratory measurements of magnetic susceptibility.

	Median	Mean	Std. dev	Max	Min
χ_{LF} ($\times 10^{-8}$ m^3 kg^{-1})	49.42	60.53	49.93	345.38	8.24
χ_{HF} ($\times 10^{-8}$ m^3 kg^{-1})	46.36	55.99	45.70	319.72	7.69
χ_{FD} Difference ($\times 10^{-8}$ m^3 kg^{-1})	3.31	4.54	4.83	43.65	0.02
χ_{FD}%	7.35	7.27	2.462	17.44	0.81

Note: Measurements were conducted on 139 samples. Standard MS practice takes low frequency (χ_{LF}) as the best measure of actual MS due to the decreased influence of small grain sizes with high frequency MS (χ_{HF}) (Dearing, 1999). While the MS values are calculated in SI units of 10^{-5} due to the low value of MS measurements, these are values corrected for the sample's masses, which are presented in 10^{-8} m^3 kg^{-1}. The 139 samples have a mean χ_{LF} of 60.53×10^{-8} m^3 kg^{-1}. 61% of the values fall below the mean, while 90% of the values have χ_{LF} values lower than 110.00×10^{-8} m^3 kg^{-1}. The final 10.00% of the MS values represents a range from 110.00×10^{-8} to 345.00×10^{-8} m^3 kg^{-1}. χ_{FD}% provides an indication of the influence of separate grain sizes on magnetic susceptibility. As shown in the table, the grain size ranges from the MD domain range (<1%) to the SP-dominated sample sizes (>7%), with the mean falling in the superparamagnetic region.

Abbreviations: MD, multidomain; MS, magnetic susceptibility.

MS metre is insufficient in measuring lower MS values (Dearing, 1999).

To mitigate the influence of systematic error, each sample was organized into groups of 10 by categorizing the strength of their χ_{LF} values, except for the last group (G14), which was composed of the nine samples with the largest values. For each group, then, the mean χ_{LF}, χ_{HF} and χ_{FD} differences, and χ_{FD}% were calculated. These results are presented in the Supporting Information Material. Figure 5c,d shows the relationship between χ_{LF} and χ_{HF} to the χ_{FD}%, respectively. In these groups, the correlation (0.203) between χ_{LF} and χ_{FD}% as well as the correlation (0.195) between χ_{HF} and χ_{FD}% are very low (Figure 5d). This indicates that an increase or decrease in the measured MS values is not likely to predict χ_{FD}%; therefore, the influence of machine-induced systemic error is low.

Using these groups, some patterns can be identified. Samples with low χ_{LF} values have the widest range of χ_{FD}%. χ_{LF} values of 50.00×10^{-8} (m^3/kg) or lower are spread out within the entire range of the χ_{FD}% (group means 5.90%–8.54%). Low χ_{LF} results seem to be characterized by varying concentrations of SD and SP grains. In contrast, moderate to high mean χ_{LF} values (60.00×10^{-8} [m^3/kg] and above) all fall above χ_{FD}% of 7.00% (Figure 6b). This indicates that as χ_{LF} values increase, there is an increase in the concentration of SP grains compared to SD grains.

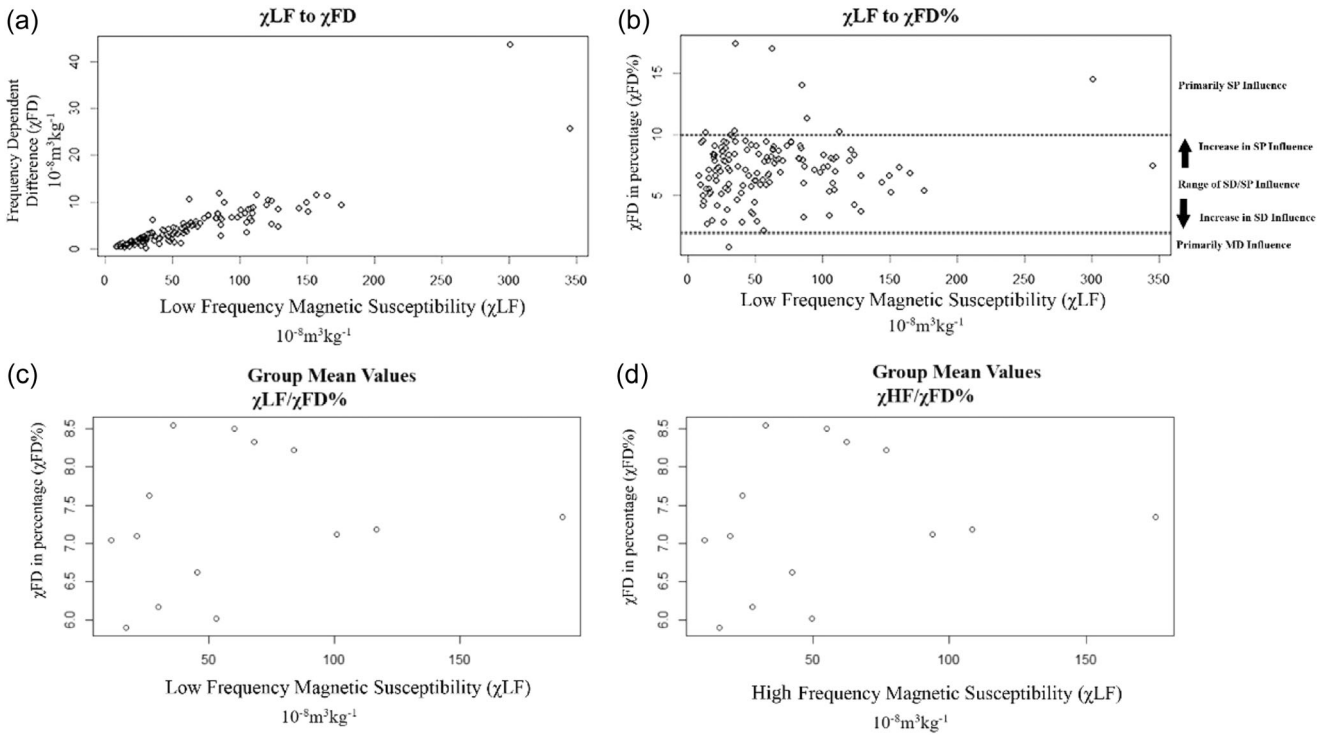

FIGURE 5 Plots showing low-frequency MS and ground low-frequency MS against others. (a) It is clear that there is a relationship between low frequency and the value of the difference between χ_{LF} and χ_{HF}. (b) It can be seen that there is little relationship between the low-frequency measurements and the percentage difference between the two frequencies. From (c) and (d), it can be seen that the relationship between low frequency and high frequency to the frequency-dependent %, respectively, is more equally correlated when the MS is grouped. The correlation between high frequency and χ_{FD}% decreases drastically, with a Pearson's correlation of 0.195. MS, magnetic susceptibility.

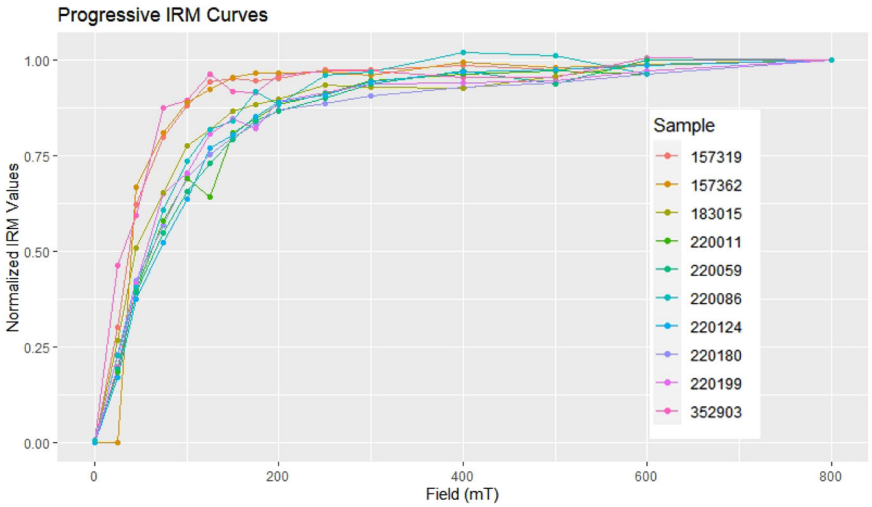

FIGURE 6 Normalized IRM curves for the 10 samples demonstrating the variation in magnetic content. Normalization of data were undertaken by dividing the IRM values by the true SIRM of the sample for a proper comparison between the IRM curves. True SIRMs are the maximum value measured IRM at 800 mT. IRM, isothermal remanent magnetization; SIRM, saturation IRM. [Color figure can be viewed at wileyonlinelibrary.com]

TABLE 3 All values measured for the samples including low-frequency MS (χ_{LF}); frequency-dependent MS (χ_{FD}%); IRM saturations at 25, 300 mT and the SIRM; the 300 mT/SIRM ratio, which compare ferrimagnetic to anti-ferrimagnetic content by showing a ratio of saturation at 300 mT to the SIRM; ARM values; and the ratio of ARM to SIRM.

Sample	$\chi_{LF} \times 10^{-8}$ m^3 kg^{-1}	χ_{FD}%	25 mT (*A/m*)	300 mT (*A/m*)	SIRM (*A/m*)	Ratio 300 mT/SIRM	Saturation % by 200 mT	ARM values (*A/m*)	ARM/SIRM
157319	49.42	6.25	2.62	8.53	8.74	0.98	95.27	0.10	0.011
157362	85.77	6.04	0.01	12.24	12.73	0.96	96.60	0.15	0.012
183015	94.04	7.12	3.02	10.47	11.26	0.93	89.99	0.11	0.009
220011	60.62	6.07	1.64	8.44	8.92	0.95	88.47	0.02	0.002
220059	42.91	7.14	1.11	5.37	5.72	0.94	86.61	0.07	0.012
220086	53.97	7.14	1.21	5.20	5.36	0.97	88.49	0.11	0.021
220124	28.15	5.62	0.69	3.80	4.03	0.94	89.09	0.03	0.008
220180	24.59	8.93	0.62	2.46	2.71	0.91	86.98	0.07	0.026
220199	156.68	7.34	3.63	17.05	18.19	0.94	89.20	0.03	0.002
352903	345.38	7.43	12.96	26.47	27.97	0.95	96.01	0.24	0.009

Abbreviations: ARM, anhysteretic remanent magnetization; IRM, isothermal remanent magnetization; MS, magnetic susceptibility; SIRM, saturation IRM.

3.2.3 | IRM and anhysteric remanent magnetization results

The IRM analysis (Figure 6, Table 3) indicates that the magnetic behaviour of all samples is primarily dominated by ferrimagnetic, magnetite or maghemite grains. On combining IRM results with χ_{FD}%, we can see that samples with higher χ_{LF} are characterized by higher concentrations of SP grains or an increase in the ferrimagnetic (*s.s.*) concentration. The highest χ_{LF} values correspond to samples with a high concentration of SP magnetite/maghemite. Figure 6 shows that all samples have 300 mT/SIRM ratios ranging from 0.91 to 0.98 (values near unity are indicative of ferrimagnetic dominance; Bloemendal et al., 1992), indicating that χ_{LF} signatures are heavily driven by ferrimagnetic material, which saturates before 300 mT. Any anti-ferrimagnetic (haematite or goethite) components, which do not saturate by 300 mT, will have very little influence upon the magnetic signature. Changes in χ_{LF} seem to be driven by variations in the concentrations of SD and SP grains, as well as variations in the concentrations of low-coercivity minerals.

Both SIRM and ARM values are influenced by grain size. The ARM/SIRM ratio can be utilized to further estimate the effect of ferrimagnetic (*s.s.*) grain sizes on the magnetic signature. An increase in ARM/SIRM values indicates a decrease in grain size (Evans & Heller, 2003). The addition of ARM/SIRM hints that grain size can play a role in altering χ_{LF} values, but not as drastically as the ferrimagnetic (*s.s.*) concentration. ARM/SIRM ratios range from 0.00155 to 0.02137. Looking at these values, we find that moderate to moderately high ARM/SIRM values of 0.009–0.012 (Table 2) can be present within moderately high χ_{LF} values, ~85×10^{-8} (m^3/kg) (Table 2: Samples 157362, 183015), as well as the highest χ_{LF} values, ~354×10^{-8} (m^3/kg) (Table 2: Sample 352903), indicating that there is at least a mixture of coarse and fine grains if not a high frequency

of moderate grain sizes. However, very high χ_{LF} values, 156×10^{-8} (m^3/kg) (Table 2: Sample 220199), can also have low ARM/SIRM values, 0.002, indicating that this signature can also be driven by relatively coarser grains. In contrast, Sample 220124 has the second lowest χ_{LF} of the measured, but an ARM/SIRM comparable to that of Sample 352903, as well as a low-coercivity concentration similar to both Samples 220199 and 352903 (300 mT/SIRM of 0.94). The primary difference between it and the other two samples is its χ_{FD}% of 5.62%, compared to 7.34% and 7.43% for Samples 220199 and 352903, respectively, indicating an increase in the SP domain size fraction. The likely explanation for the increase in MS values is the influence of an increased concentration of magnetite. Considering that an increase in χ_{LF} values correlates to an increase in χ_{FD}%, the higher χ_{LF} values are characterized by higher concentrations of SP-sized magnetite/maghemite, which is in agreement with other studies at South African sites (Herries, 2006, 2009; Herries & Fisher, 2010).

4 | DISCUSSION

4.1 | ALBS and SADBS

The age model for PP5-6N dates ALBS and SADBS between 74 and 71 ka (Smith et al., 2018). Coastline reconstruction shows that during the ALBS and SADBS, the cave's distance from the coastline was between 1.7 and 22.0 km. This large variation is due to the shift from MIS5 to 4, which saw a drop in sea levels and a heavy coastline retreat across the South African Agulhas Bank. The ALBS is an aeolian dune that forms as the coast begins its retreat, thus providing a source for the sand (Fisher et al., 2010; Karkanas et al., 2015). The SADBS is a continuation of the same MIS4 deposition as the ALBS. However, the archaeological deposits and combustion features are far denser, a cumulative palimpsest, indicating a greater and consistent occupation of this area of the site (Karkanas et al., 2015).

The mapping of the magnetic in situ susceptibility can be divided into five areas of unique IMS patterning. The lowest of these areas ranges from elevations of 18.8–19.8 masl (see Figures 2e and 3b) and aligns with the stratigraphic subaggregate called the 'Conrad Cobble and Sand' (Smith et al., 2018). This area is characterized by a mottled composition of low to moderate IMS values. Previous experimental work on associated dune sands from Pinnacle Point has indicated that these sands are primarily composed of diamagnetic quartz material (Herries & Fisher, 2010; SOM), and it has been indicated that these aeolian deposits are relatively unaltered by chemical processes (Karkanas et al., 2015). Therefore, it can be expected that the aeolian deposits of the 'Conrad Cobble and Sand' should have uniformly low IMS values. However, the deposits are mottled, with moderate IMS values (i.e., between 19.4 and 19.5 m in Figure 3b). A likely factor responsible for the mottling of moderate values is anthropogenic inputs within these deposits. However, there are no visible combustion features within this deposit to explain the enhancement of the IMS. One hypothesis is that these values represent the outskirts of a much denser occupation occurring elsewhere on the site. Movement of the site's occupants could spread ash material from combustion features, carried on the bottom of their feet, throughout the site. This depositional action may also have occurred at PP13B and coincides with micromorphological evidence for trampling here at PP5-6N (Herries & Fisher, 2010; Karkanas et al., 2015). Against the backdrop of a low MS dune sand, these actions would be visible and provide evidence for more intense occupation occurring elsewhere on the site (Herries & Fisher, 2010). Magnetic mineralogical analysis in the laboratory shows that moderate MS values do correlate with an increase in the χ_{FD}% and the overall concentration of SP grains. At Pinnacle Point, increases in χ_{FD}% have been associated with an increase in fine-grain ferrimagnetic minerals associated with burnings (Herries & Fisher, 2010), and this could be further evidence that anthropogenic fires were being utilized elsewhere on the site. The IMS evidence alone does not prove this hypothesis. However, interpretation by Karkanas et al. (2015) of the microscopic structure of the ALBS' aeolian deposits does not align with other dune deposits at Pinnacle Point. The ALBS aeolian deposits show evidence of flattening through human occupation that could be an intentional action, but also occur through trampling of the deposits (Karkanas et al., 2015). Furthermore, these aeolian deposits have been noted to have ephemeral lenses of anthropogenic deposits (Smith et al., 2018). Combined with this evidence, the moderate IMS values appear to reinforce this idea of anthropogenically influenced deposits through activities elsewhere on the site.

Above the 'Conrad Cobble and Sand', the 'Conrad Shell' is the most prominent anthropogenic evidence in the ALBS (see Figures 2e and 3b, from elevations of 19.8–20 masl). The 'Conrad Shell' is composed of almost uniformly high IMS values, with only a few areas showing lower moderate values. Micromorphological interpretation of the 'Conrad Shell' shows it as a sequence composed of white ash MF and sand-rich ash MF with clear faunal remains, primarily whole shells, and some burnt bone (Karkanas et al., 2015). The 'Conrad Shell' is composed of high IMS values expected from a combustion feature, making it difficult to interpret much in the model's patterning. The white ash and sand-rich ash MF have been associated with bioturbation (Karkanas et al., 2015), and this could be one explanation for the pockets of moderate IMS values and disruption in the homogeneity of the high IMS values. The mineralogical assessment conducted in our laboratory finds that high MS values, as those presented in the combustion feature, are composed of magnetite/maghemite with increasing concentrations of fine SP grains compared to the SD grain component. Experimental fires conducted on Pinnacle Point's aeolian dune sands by Herries and Fisher (2010) indicate that the repeated burnings on the same sediment will produce an increase in χ_{FD}% values. However, excessive burnings, at a minimum of four repeated burns of the same combustion feature, will eventually lower the χ_{FD}, to ~8% (Herries & Fisher, 2010), as SP grains are converted into ultra-fine SP grains, and no longer contribute to the overall MS. As the underlying low magnetic aeolian sand sedimentary sequence is low in organic

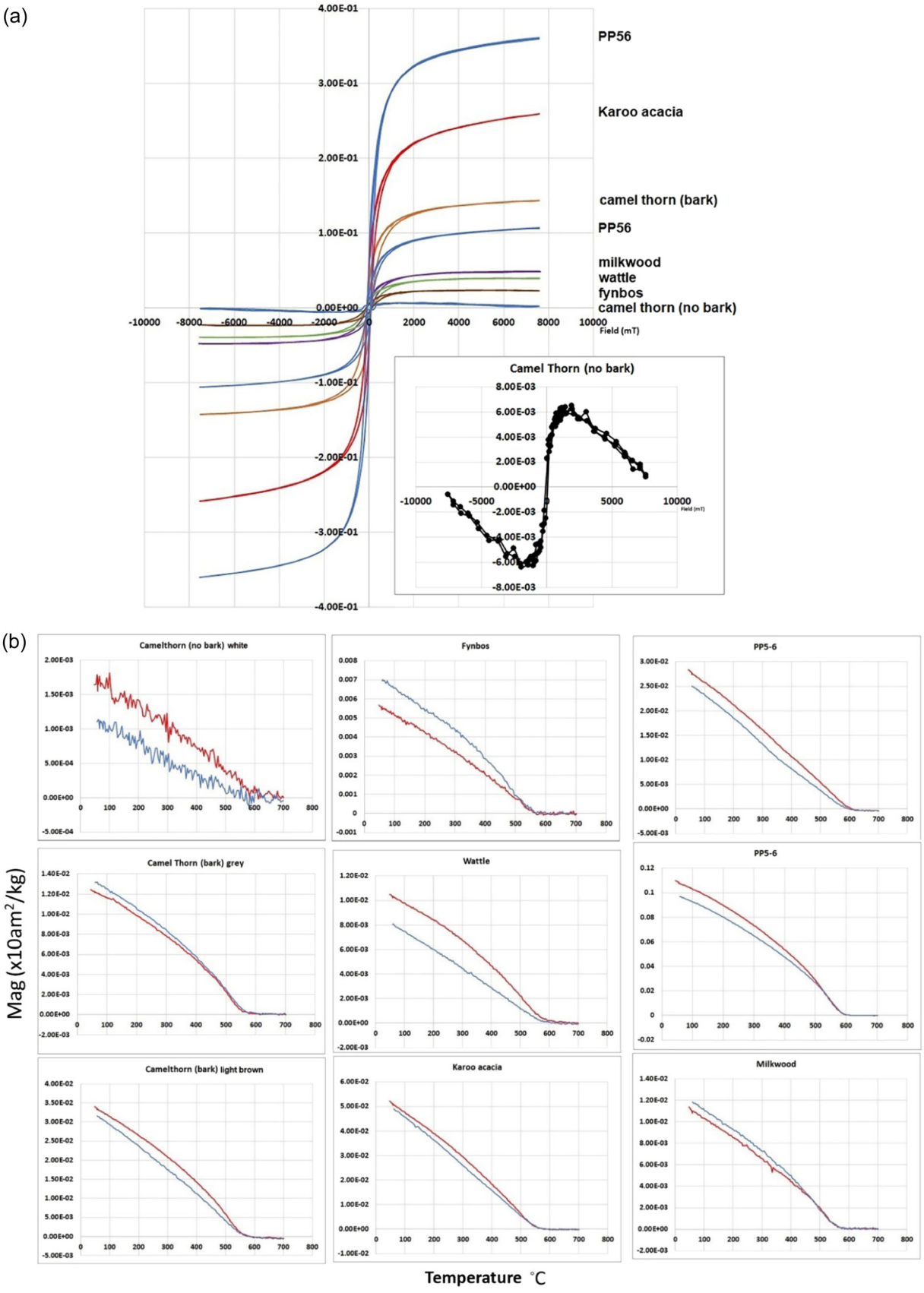

FIGURE 7 (See caption on next page)

material and infrequent in iron-bearing components, this increase can be attributed partially to the enhancement of this infrequent iron component, but is primarily driven by the introduction of the ash component. Ash has previously been shown to be a strong source of magnetic minerals in combustion features (McClean & Church et al., 2007; McClean & Kean, 1993). Wood-ash experimental work from Pinnacle Point shows that different species of trees created ash of different magnetic enhancements; thick-barked species produced the ash with the highest values (Figure 7 and Supporting Information Material). In contrast, ash made from wood without bark was magnetically weak (Figure 7 and Supporting Information Material). If different wood species, or even Dicot leaves, were used as a fuel source (Albert & Marean, 2012) throughout the PP 5-6 sequence, then this could significantly affect the magnetic signature. Phytoliths from SADBS indicate a dominance of Dicot species and leaves in these deposits, compared to potentially different species in the older ALBS; however, phytolith numbers were extremely low in ALBS (Esteban et al., 2020). The experiments conducted by Herries and Fisher (2010) utilized a wood species (Red-Eyed Wattle) that created magnetically strong ash. As such, the significant enhancement was thought to be partly driven by increasing ash content as it became mixed into the sediments with repeated burning (Herries & Fisher, 2010). Measurements through the sediment have shown that any enhancement from burning was limited to a few centimetre below the combustion event and was therefore not a product of postdepositional heating from above. A significant increase (8%) occurred in the χ_{FD}% after a single firing, increasing to a maximum (~12%) after three firings and decreasing (to 8%) after four firings (Herries & Fisher, 2010). This pattern correlates with a pattern noted in sites across South Africa whereby in situ hearths often have a very high MS but lower χ_{FD}% values than mixed anthropogenic sediments (Herries, 2009; Herries & Fisher, 2010). The χ_{LF} and χ_{FD}% here correspond to the experimental results of Herries and Fisher (2010) for multiple burnings. Previous magnetic mineralogical assessment conducted at the Pinnacle Point cave complex (Herries & Fisher, 2010, SOM) as well as experimental analysis along with reference measurements conducted on deposits from elsewhere at PP5-6N (Figure 7, also see Supporting Information Material) indicate that the likely driver of this signature is magnetite. However, this is yet to be demonstrated for the ALBS and SADBS.

Above the 'Conrad Shell', the 'Conrad Sand' represents the final ALBS deposit (see Figure 2d; in Figure 4b elevations at 20.4–20.65 masl). Like the 'Conrad Cobble and Sand', the 'Conrad Sand' is composed of a large deposit of aeolian sands. However, unlike the lower deposits, the 'Conrad Sand' is characterized by uniformly low IMS values. The low MS here is likely a product of minimal anthropogenic input relative to sedimentation during the final stages of the ALBS.

Above the 'Conrad Sand' is the SADBS. In the IMS models, the SADBS can be divided into two areas: a lower SADBS unit, Jocelyn, (see Figure 2d, in Figure 4, elevations of 20.65–20.95 masl) and an upper SADBS, Erich (see Figure 2d, in Figure 4, elevations of 20.95–21.2 masl). Overall, the SADBS is characterized by an increase in the intensity of anthropogenic deposition and a cumulative palimpsest of combustion features (Karkanas et al., 2015). In Jocelyn, the SADBS has a more mottled appearance, with IMS values ranging from low to moderate values of ~40×10^{-8} $m^3 kg^{-1}$ to high values of ~143×10^{-8} $m^3 kg^{-1}$. The high values appear in two fragmented horizons (as discussed in our Section 3). This lower component of the SADBS is described as having a high sand frequency, which likely accounts for the mottled low to moderate values, with the overall patterning being a byproduct of bioturbated disturbance of the deposit. However, the fragmented horizons of high IMS values could indicate areas where the original deposits are archaeologically intact and remain within their original depositional context. In the upper SADBS deposit of Erich, the IMS values are much more uniformly high, which is potentially due to less disruption by bioturbating processes.

The SADBS contains the highest IMS values within this study, with the highest values exceeding 300×10^{-5} (S.I. units). As with the 'Conrad Shell' combustion feature, the SADBS contains evidence for multiple burnings. This is visible in the micromorphology interpretations, which describe the extensiveness and density of the combustion features, making it difficult to isolate single instances of hearths within the deposits, and forming a cumulative palimpsest. The micromorphological analysis of these combustion features shows good evidence for the preservation of the ash component, with little evidence for diagenetic reworking or recrystallization of these components (Karkanas et al., 2015). The likely disturbances to these deposits are from the trampling of the features, and not through later diagenetic alterations (Karkanas et al., 2015). The sandy ash MF have more evidence for bioturbation while retaining evidence for ash crystals (Karkanas et al., 2015). The overall preservation of the combustion features in Erich, as well as the components of Jocelyn that are visibly intact, helps reinforce the interpretation that these higher IMS values are reflective of the magnetic mineralogical conditions after their use. As discussed with the 'Conrad Shell' combustion feature, these high IMS values, along with associated χ_{FD}% of ~8%, are in alignment with experimental results for multiple burnings as identified by Herries and Fisher (2010). The potential that these combustion features were exposed to multiple

FIGURE 7 Results of experimental reference samples demonstrating the difference in potential magnetization of combustion fuel sources located around the site and two comparative samples from Pinnacle Point 5-6 (not associated with ALBS and SADBS). (a) Hysteresis Loops demonstrating the variability in magnetization between the various fuel sources around the site. Of particular interest is the comparison between Camel Thorn (no bark) and Camel Thorn (bark), highlighting that a portion of the magnetic mineral input is carried in the bark of this fuel source. (b) Thermomagnetic curves of samples showing demagnetization at around ~600°C, indicating a primary driver of magnetite within the experimental reference samples. See the Supporting Information Material for more details. ALBS, Ashy Light Brown Sand; SADBS, Shelly Ashy Dark Brown Sand

episodes of burning could be representative of a more intense and sustained period of occupation compared to what was below it in the ALBS, or at least a more intensive use of this area of PP5-6N.

4.2 | Viability of modelling in the field

Spatial modelling of in situ MS has provided insight into stratigraphic characteristics that may not be entirely visible to a macroscopic investigation. In the field, the creation of the models requires a set of specialized equipment: total stations; IMS metres, a camera capable of colour-corrected photography, along with computers, software and the know-how to reliably collect the data, process these and generate the models. Much of this equipment is now relatively standard for modern archaeological excavations, while basic MS field metres are relatively inexpensive, notwithstanding the specialists with the know-how to operate and interpret these data.

If access to the equipment is available, then generating the models can be relatively quick. For moderate-resolution sampling of the ALBS wall sections, ~1 m in width and 1.2 m in height, half a field day was required to measure with a 2–3-person team to operate the total station and record the results. The creation of georectified photos of the section with an appropriate set-up took only a few hours longer, albeit at night, to control for light sources (Fisher et al., 2015). The modelling was dependent upon the complexity of the data and fine-tuning using cross-validation statistics, which usually took 6–8 h depending on the section.

The primary obstacle is interpretive and not technical. The methodology used here involved a team that is experienced in interdisciplinary collaboration and a shared understanding of all the methods being used. Understanding what the variations within the IMS model show involves not only understanding what changes in MS may mean but how these relate to both the geological and anthropogenic contexts of the changes. This requires an interdisciplinary approach.

In our study, we utilized the laboratory analysis of magnetic mineralogy from stratigraphically associated bulk sediment samples to provide contextual magnetic data for the results. These laboratory results have provided greater insight into these magnetic characteristics and have helped drive our interpretations. Furthermore, we have associated our models with the micromorphological interpretations of the SADBS and ALBS (see Karkanas et al., 2015), which has greatly improved the interpretations of these models.

An increased interdisciplinary analysis will only improve the interpretive potential of these models. Future avenues of research should focus on more deeply integrating analysis of laboratory magnetic mineralogy and micromorphology with the IMS models, preferably by being able to connect these methods through shared use of samples and direct sampling of the profile. Further interdisciplinary methods to improve the interpretive potential of these models could include the integration of artefact density data as presented in Wilkins et al. (2017) and Smith et al. (2018) and the analysis of cryptotephra (Smith et al., 2018), as well as lateral 3D spatial analysis of magnetic mineralogy as conducted by Herries and Fisher (2010). As interdisciplinary integration increases, interpretation of anthropogenic influence will improve and help identify human behaviour more readily identifiable within the IMS models.

5 | CONCLUSIONS

At the outset of this paper, we aimed to demonstrate that there is a consistent variation in the magnetic signature of ALBS and SADBS, which is driven by changes to the magnetic mineralogical and granulometry composition of the studied areas; that these changes in mineralogical composition are primarily influenced by anthropogenic actions; that our models can be used to map the changes in mineralogy as well as identify geogenic and anthropogenic features; that with the assistance of laboratory analysis, the models can explore if the variation in the presence or absence of anthropogenic material in a sequence is due to changes in occupational intensity, or due to changes in the areas of the site being utilized; that these data can be used in association with other data generated on-site to interpret patterns of human behaviour; and the models correlate well with micromorphological interpretations of the site.

The models for ALBS and SADBS reflect changes in occupational behaviour at the site. This can be interpreted as changes in when and how intensely the site was being occupied. However, results can also be interpreted as changes in what parts of the site were being occupied, with changes from moderate to high IMS values reflecting how close the main activity area was to the modelled locations. Laboratory analysis of associated bulk sediment samples shows that increasing MS values are associated with an increase in concentrations of ferrimagnetic (magnetite/maghemite) minerals, along with the increased concentration of SP grains associated with anthropogenic fire use. Finally, our models correlate well with previously published micromorphological and artefact density data at the site (Karkanas et al., 2015; Smith et al., 2018), while providing a unique insight into stratigraphic changes within the ALBS and SADBS at Pinnacle Point 5-6N.

ACKNOWLEDGEMENTS

The authors acknowledge the support through grants of the National Science Foundation (BCS-0524087, BCS-1138073 and BCS-1460376), Hyde Family Foundations, the Institute of Human Origins (IHO) at Arizona State University and the John Templeton Foundation to the Institute of Human Origins at Arizona State University; as these organizations supported the excavations at PP5-6N. Funding for the magnetic analysis was provided by the Australian Research Council Future Fellowship FT120100399 to AIRH. The opinions expressed in this publication are those of the author(s) and do not necessarily reflect the views of any of these funding organizations. The authors would also like to extend our gratitude to the editors at Geoarchaeology and those who reviewed this submission. Their insights have greatly improved this paper. Open access publishing facilitated by La Trobe University, as part of the Wiley - La Trobe University agreement via the Council of Australian University Librarians.

DATA AVAILABILITY STATEMENT

The data that support the findings of this study are available in the article or provided in the Supporting Information Material of this article.

ORCID

Ada Dinckal http://orcid.org/0000-0001-6570-7793
Curtis W. Marean http://orcid.org/0000-0002-2670-5733

REFERENCES

Albert, R. M., & Marean, C. W. (2012). The exploitation of plant resources by early *Homo sapiens*: The Phytolith Record from Pinnacle Point 13B Cave, South Africa. *Geoarchaeology*, *27*(4), 363–384. https://doi.org/10.1002/gea.21413

Bar-Matthews, M., Marean, C. W., Jacobs, Z., Karkanas, P., Fisher, E. C., Herries, A. I. R., Brown, K., Williams, H. M., Bernatchez, J., Ayalon, A., & Nilssen, P. J. (2010). A high resolution and continuous isotopic speleothem record of paleoclimate and paleoenvironment from 90 to 53 ka from Pinnacle Point on the south coast of South Africa. *Quaternary Science Reviews*, *29*(17–18), 2131–2145. https://doi.org/10.1016/j.quascirev.2010.05.009

Bloemendal, J., King, J. W., Hall, F. R., & Doh, S.-J. (1992). Rock magnetism of Late Neogene and Pleistocene deep-sea sediments: Relationship to sediment source, diagenetic processes, and sediment lithology. *Journal of Geophysical Research: Solid Earth*, *97*(B4), 4361–4375. https://doi.org/10.1029/91JB03068

Bradák, B., Carrancho, Á., Herrejón Lagunilla, Á., Villalaín, J. J., Monnier, G. F., Tostevin, G., Mallol, C., Pajović, G., Baković, M., & Borovinić, N. (2020). Magnetic fabric and archaeomagnetic analyses of anthropogenic ash horizons in a cave sediment succession (Crvena Stijena site, Montenegro). *Geophysical Journal International*, *224*(2), 795–812. https://doi.org/10.1093/gji/ggaa461

Brown, K. S., Marean, C. W., Herries, A. I., Jacobs, Z., Tribolo, C., Braun, D., Roberts, D. L., Meyer, M. C., & Bernatchez, J. (2009). Fire as an engineering tool of early modern humans. *Science*, *325*(5942), 859–862. https://doi.org/10.1126/science.1175028

Brown, K. S., Marean, C. W., Jacobs, Z., Schoville, B. J., Oestmo, S., Fisher, E. C., Bernatchez, J., Karkanas, P., & Matthews, T. (2012). An early and enduring advanced technology originating 71,000 years ago in South Africa. *Nature*, *491*(7425), 590–593. https://doi.org/10.1038/nature11660

Carrancho, Á., & Villalaín, J. J. (2011). Different mechanisms of magnetisation recorded in experimental fires: Archaeomagnetic implications. *Earth and Planetary Science Letters*, *312*(1–2), 176–187. https://doi.org/10.1016/j.epsl.2011.10.006

Carrancho, Á., Villalaín, J. J., Angelucci, D. E., Dekkers, M. J., Vallverdú, J., & Vergès, J. M. (2009). Rock-magnetic analyses as a tool to investigate archaeological fired sediments: A case study of Mirador cave (Sierra de Atapuerca, Spain). *Geophysical Journal International*, *179*(1), 79–96. https://doi.org/10.1111/j.1365-246X.2009.04276.x

Carrancho, Á., Villalaín, J. J., Vergès, J. M., & Vallverdú, J. (2012). Assessing post-depositional processes in archaeological cave fires through the analysis of archaeomagnetic vectors. *Quaternary International*, *275*, 14–22. https://doi.org/10.1016/j.quaint.2012.01.010

Church, M. J., Peters, C., & Batt, C. M. (2007). Sourcing fire ash on archaeological sites in the Western and Northern Isles of Scotland, using mineral magnetism. *Geoarchaeology*, *22*(7), 747–774. https://doi.org/10.1002/gea.20185

Crowther, J., Macphail, R. I., & Cruise, G. M. (1996). Short-term, post-burial change in a humic rendzina soil, overton down experimental earthwork, Wiltshire, England. *Geoarchaeology*, *11*(2), 95–117. https://doi.org/10.1002/(sici)1520-6548(199603)11:2<95::Aid-gea1>3.0.Co;2-4

Curnoe, D., Xueping, J., Herries, A. I. R., Kanning, B., Taçon, P. S. C., Zhende, B., Fink, D., Yunsheng, Z., Hellstrom, J., Yun, L., Cassis, G., Bing, S., Wroe, S., Shi, H., Parr, W. C. H., Shengmin, H., & Rogers, N. (2012). Human remains from the Pleistocene-Holocene transition of Southwest China suggest a complex evolutionary history for East Asians. *PLoS One*, *7*(3), e31918. https://doi.org/10.1371/journal.pone.0031918

Dearing, J. A. (1994). *Environmental magnetic susceptibility: Using the Bartington MS2 System*. Chi Publications.

Dearing, J. A. (1999). Magnetic susceptibility. In J. Walden, F. Oldfield, & J. P. Smith (Eds.), *Environmental magnetism: A practical guide* (pp. 25–62). Quaternary Research Association.

Dearing, J. A., Dann, R. J. L., Hay, K., Lees, J. A., Loveland, P. J., Maher, B. A., & O'Grady, K. (1996a). Frequency-dependent susceptibility measurements of environmental materials. *Geophysical Journal International*, *124*(1), 228–240. https://doi.org/10.1111/j.1365-246X.1996.tb06366.x

Dearing, J. A., Hay, K. L., Baban, S. M. J., Huddleston, A. S., Wellington, E. M. H., & Loveland, P. J. (1996b). Magnetic susceptibility of soil: An evaluation of conflicting theories using a national data set. *Geophysical Journal International*, *127*(3), 728–734. https://doi.org/10.1111/j.1365-246X.1996.tb04051.x

Dunlop, D. J., & Ozdemir, O. (1997). *Rock Magnetism: Fundamentals and frontiers*. Cambridge University Press.

Esteban, I., Marean, C. W., Cowling, R. M., Fisher, E. C., Cabanes, D., & Albert, R. M. (2020). Palaeoenvironments and plant availability during MIS 6 to MIS 3 on the edge of the Palaeo-Agulhas Plain (south coast, South Africa) as indicated by phytolith analysis at Pinnacle Point. *Quaternary Science Reviews*, *235*, 105667. https://doi.org/10.1016/j.quascirev.2019.02.022

Evans, M., & Heller, F. (2003). *Environmental magnetism: Principles and applications of enviromagnetics*. Academic Press.

Fisher, E. C., Akkaynak, D., Harris, J., Herries, A. I. R., Jacobs, Z., Karkanas, P., Marean, C. W., & McGrath, J. R. (2015). Technical considerations and methodology for creating high-resolution, color-corrected, and georectified photomosaics of stratigraphic sections at archaeological sites. *Journal of Archaeological Science*, *57*, 380–394. https://doi.org/10.1016/j.jas.2015.02.022

Fisher, E. C., Bar-Matthews, M., Jerardino, A., & Marean, C. W. (2010). Middle and Late Pleistocene paleoscape modeling along the Southern coast of South Africa. *Quaternary Science Reviews*, *29*(11–12), 1382–1398. https://doi.org/10.1016/j.quascirev.2010.01.015

Goldberg, P., & Macphail, R. I. (2012). Gorham's Cave sediment micromorphology. In R. N. E. Barton, C. B. Stringer, & J. C. Finlayson (Eds.), *Neanderthals in Context: A report of the 1995-1998 excavations at Gorham's and Vanguard Caves, Gibraltar* (pp. 50–61). Oxford University School of Archaeology.

Herrejón Lagunilla, Á., Carrancho, Á., Villalaín, J. J., Mallol, C., & Hernández, C. M. (2019). An experimental approach to the preservation potential of magnetic signatures in anthropogenic fires. *PLoS One*, *14*(8), e0221592. https://doi.org/10.1371/journal.pone.0221592

Herries, A. I. R. (2006). Archaeomagnetic evidence for climate change at Sibudu Cave. *South African Humanities*, *18*(1), 131–147.

Herries, A. I. R. (2009). New approaches for integrating palaeomagnetic and mineral magnetic methods to answer archaeological and geological questions on Stone Age sites. In A. Fairbairn, S. O'Connor, & B. Marwick (Eds.), *New directions in archaeological science* (pp. 235–254). ANU E Press.

Herries, A. I. R. (2018). Archaeomagnetic analysis of sediments from Djadjiling Rockshelter (HD07-1A-04), Pilbara, Western Australia. In D. Cropper, & W. B. Law (Eds.), *Rockshelter excavations in the East Hamersley Range, Pilbara Region, Western Australia*. Archaeopress.

Herries, A. I. R., & Fisher, E. C. (2010). Multidimensional GIS modeling of magnetic mineralogy as a proxy for fire use and spatial patterning: Evidence from the Middle Stone Age bearing sea cave of Pinnacle

Point 13B (Western Cape, South Africa). *Journal of Human Evolution*, *59*(3–4), 306–320. https://doi.org/10.1016/j.jhevol.2010.07.012

Hofmann, D., Fabian, K., Schmieder, F., Donner, B., & Bleil, U. (2005). A stratigraphic network across the subtropical front in the central South Atlantic: Multi-parameter correlation of magnetic susceptibility, density, X-ray fluorescence and δ18O records. *Earth and Planetary Science Letters*, *240*(3–4), 694–709. https://doi.org/10.1016/j.epsl.2005.09.048

Herries, A. I. R., & Latham, A. G. (2009). Archaeomagnetic studies at the Cave of Hearths. In J. McNabb & A. G. M. Sinclair (Eds.), *The Cave of Hearths: Makapan' Middle Pleistocene research project* (Vol. 1., pp. 59–64). Archaeopress.

Bartington Instruments. (2019). *Operation manual for MS2 magnetic susceptibility system*. GMW Associates.

Jacobs, Z. (2010). An OSL chronology for the sedimentary deposits from Pinnacle Point Cave 13B—A punctuated presence. *Journal of Human Evolution*, *59*(3–4), 289–305. https://doi.org/10.1016/j.jhevol.2010.07.010

Jordanova, N., Jordanova, D., Barrón, V., Lesigyarski, D., & Kostadinova-Avramova, M. (2019). Rock-magnetic and color characteristics of archaeological samples from burnt clay from destructions and ceramics in relation to their firing temperature. *Archaeological and Anthropological Sciences*, *11*(7), 3595–3612. https://doi.org/10.1007/s12520-019-00782-y

Karkanas, P., Brown, K. S., Fisher, E. C., Jacobs, Z., & Marean, C. W. (2015). Interpreting human behavior from depositional rates and combustion features through the study of sedimentary microfacies at site Pinnacle Point 5-6, South Africa. *Journal of Human Evolution*, *85*, 1–21. https://doi.org/10.1016/j.jhevol.2015.04.006

Kukkonen, I. T., Meiettinen, M., Julkunen, A., & Mattson, A. (1997). Magnetic prospecting of Stone Age red ochre graves with a case study from Laukaa, Central Finland. *Fennoscandia Archaeologica, XIV*, 3–22.

Liu, Q., Roberts, A. P., Larrasoaña, J. C., Banerjee, S. K., Guyodo, Y., Tauxe, L., & Oldfield, F. (2012). Environmental magnetism: Principles and applications. *Reviews of Geophysics*, *50*(4). https://doi.org/10.1029/2012rg000393

Macphail, R. I., & Crowther, J. (2007). [Special section on the Yiluo project] soil micromorphology, chemistry and magnetic susceptibility studies at Huizui (Yilou Region, Henan Province, Northern Chine), with special focus on a typical Yangshao floor sequence. *Bulletin of the Indo-Pacific Prehistory Association*, *27*, 101–103. https://doi.org/10.7152/bippa.v27i0.11981

Macphail, R. I., Crowther, J., Acott, T. G., Bell, M. G., & Cruise, J. M. (2003). The experimental earthwork at Wareham, dorset after 33 years: Changes to the buried LFH and Ah Horizons. *Journal of Archaeological Science*, *30*(1), 77–93. https://doi.org/10.1006/jasc.2002.0823

Maher, B. A. (1998). Magnetic properties of modern soils and quaternary loessic paleosols: Paleoclimatic implications. *Palaeogeography, Palaeoclimatology, Palaeoecology*, *137*(1–2), 25–54. https://doi.org/10.1016/s0031-0182(97)00103-x

Marean, C. W., Bar-Matthews, M., Bernatchez, J., Fisher, E., Goldberg, P., Herries, A. I., Jacobs, Z., Jerardino, A., Karkanas, P., Minichillo, T., Nilssen, P. J., Thompson, E., Watts, I., & Williams, H. M. (2007). Early human use of marine resources and pigment in South Africa during the Middle Pleistocene. *Nature*, *449*(7164), 905–908. https://doi.org/10.1038/nature06204

Marean, C. W., Nilssen, P. J., Brown, K., Jerardino, A., & Stynder, D. (2004). Paleoanthropological investiations of Middle Stone Ae sites at Pinnacle Point, Mossel Bay (South Africa): Archaeology and hominid remains from 2000 Field season. *Paleoanthropology*, *2*(1).

McClean, R. G., & Kean, W. F. (1993). Contributions of wood ash magnetism to archaeomagnetic properties of fire pits and hearths. *Earth and Planetary Science Letters*, *119*(3), 387–394. https://doi.org/10.1016/0012-821X(93)90146-Z

Ozán, I. L., Méndez, C., Oriolo, S., Orgeira, M. J., Tripaldi, A., & Vásquez, C. A. (2019). Depositional and post-depositional processes in human-modified cave contexts of west-central Patagonia (Southernmost South America). *Palaeogeography, Palaeoclimatology, Palaeoecology*, *532*, 109268.

Robertson, D. J., & France, D. E. (1994). Discrimination of remanence-carrying minerals in mixtures, using isothermal remanent magnetisation acquisition curves. *Physics of the Earth and Planetary Interiors*, *82*(3–4), 223–234. https://doi.org/10.1016/0031-9201(94)90074-4

Shipton, C., Roberts, P., Archer, W., Armitage, S. J., Bita, C., Blinkhorn, J., Courtney-Mustaphi, C., Crowther, A., Curtis, R., Errico, F., Douka, K., Faulkner, P., Groucutt, H. S., Helm, R., Herries, A. I. R., Jembe, S., Kourampas, N., Lee-Thorp, J., Marchant, R., … Boivin, N. (2018). 78,000-Year-old record of Middle and Later stone age innovation in an East African tropical forest. *Nature Communications*, *9*(1), 1832. https://doi.org/10.1038/s41467-018-04057-3

Smith, J. P. (1999). An introduction to the magnetic properties of natural materials. In J. Walden, F. Oldfield, & J. P. Smith (Eds.), *Environmental magnetism: A practical guide* (pp. 5–25). Quaternary Research Association.

Smith, E. I., Jacobs, Z., Johnsen, R., Ren, M., Fisher, E. C., Oestmo, S., Wilkins, J., Harris, J. A., Karkanas, P., Fitch, S., Ciravolo, A., Keenan, D., Cleghorn, N., Lane, C. S., Matthews, T., & Marean, C. W. (2018). Humans thrived in South Africa through the Toba eruption about 74,000 years ago. *Nature*, *555*(7697), 511–515. https://doi.org/10.1038/nature25967

Tauxe, L. (2010). *Essentials of rock and paleomagnetism*. University of California Press. https://doi.org/10.1525/9780520946378

Team R. Contributors. (2021). R: A Language and Environment for Statistical Computing. https://www.R-project.org/

Thompson, R., & Oldfield, F. (1986). *Environmental magnetism*. Allen & Unwin.

Wickham, H. (2016). *ggplot2: Elegant graphics for data analysis*. Springer-Verlag. https://ggplot2.tidyverse.org

Wilkins, J., Brown, K. S., Oestmo, S., Pereira, T., Ranhorn, K. L., Schoville, B. J., & Marean, C. W. (2017). Lithic technological responses to Late Pleistocene glacial cycling at Pinnacle Point Site 5-6, South Africa. *PLoS One*, *12*(3), 0174051. https://doi.org/10.1371/journal.pone.0174051

SUPPORTING INFORMATION

Additional supporting information can be found online in the Supporting Information section at the end of this article.

How to cite this article: Dinckal, A., Fisher, E. C., Herries, A. I. R., & Marean, C. W. (2022). Mapping magnetism: Geophysical modelling of stratigraphic features by using in situ magnetic susceptibility measurements at Pinnacle Point 5-6 North, South Africa. *Geoarchaeology*, 37, 840–857. https://doi.org/10.1002/gea.21924